J Polym Res (2014) 2014:406
DOI 10.1007/s10965-014-0406-7

ORIGINAL PAPER

Structure and sorption properties of hypercrosslinked polystyrenes and magnetic nanocomposite materials based on them

Alexander V. Pastukhov · Vadim A. Davankov · Vladimir V. Volkov · Sergei V. Amarantov · Kseniya I. Lubentsova

Received: 25 October 2013 / Accepted: 2 March 2014 / Published online: 15 March 2014

Abstract By using transition electron microscopy, X-ray diffraction and small-angle X-ray scattering technique porous structure of a series of polystyrene-type sorbents (microporous and biporous hypercrosslinked polystyrenes, mesoporous sorbent XAD-4) was investigated, as well as sizes of iron oxide nanoparticles introduced into their matrix. Nanocomposite sorbents have low density, a large inner surface area, and like the parent polymers, exhibit marked adsorption properties, e.g. take up from saturated vapors 1.4 g/g of iodine or 0.8 g/g chloropicrin. A general method for processing scattering data from polydisperse multicomponent systems, like the above nanocomposites, was suggested. A rather homogeneous distribution of scattering heterogeneities with radius around 3 nm was found to be characteristic of microporous hypercrosslinked polystyrenes. Radius of magnetic iron oxide (magnetite) nanoparticles varies in ranges of 2.1±0.6 nm and 6.7±3.8 nm for the above microporous and biporous hypercrosslinked polymers, while in the XAD-4 particles of all sizes from 1 to 10 nm are presented.

Keywords Hypercrosslinked polystyrene · Polymer-inorganic nanocomposites · Magnetic sorbents · Transmission electron microscopy · Iron oxides · Small-angle X-ray scattering

A. V. Pastukhov (✉) · V. A. Davankov · K. I. Lubentsova
A. N. Nesmeyanov Institute of Organoelement Compounds, Russian Academy of Sciences, ul. Vavilova 28, Moscow 119991, Russia
e-mail: avpast@gmail.com

V. V. Volkov · S. V. Amarantov
A. V. Shubnikov Institute of Crystallography, Russian Academy of Sciences, Leninskii pr. 59, Moscow 119333, Russia

Introduction

One of perspective directions of current nanotechnology is the design of hybrid materials that are provided with a desired complex of optical, electric, magnetic or semi-conductor properties. A variety of such nanocomposite materials can be obtained by generating nanodisperse inorganic insertions within a homogeneous or macroporous polymer matrix [1].

In this manner, polymeric adsorbing materials can be provided with magnetic properties, which can open new possibilities for recovering of spent sorbents by means of their magnetic separation. The latter technique was proven to be an efficient and facile procedure, e.g. in water purification [2–4]. Magnetic sorbents should be particularly convenient for processing slurry-type media such as microbiologic culture liquids. Magnetic haemocompatible adsorbents were even suggested for extracorporeal detoxification of blood [5, 6]. Materials of that type result from covering small particles of magnetite first with a layer of carbon or nanodispersed oxides of silicium, alumina or zirconium and then with a layer of a haemocompatible natural polymer as dextrane, gelatine, albumine or a synthetic polymer [6, 7]. Synthesis and properties of magnetic hydrophilic polymers based on polystyrene and polyacrylamide latexes were described [8].

Introduction of magnetic iron oxides into the matrix of strong base anion exchanging styrene copolymers of the type of Amberlite IRA-900 was subject of several patents, e.g. [9]. These products are aimed at treatment of potable and waste waters. Magnetic materials based on macroporous and gel-type polystyrene copolymers Dow 3N, XFS4195, C-100, C-145, Diphonix, IRC718 manufactured by Dow, Purolite and others were found to efficiently remove traces of copper and zinc ions from natural and industrial waters [10]. Cobalt and nickel contaminated waste waters can be processed with polyacryl amide-type resins provided with magnetite inclusions [11].

Structure of composites obtained by the precipitation of iron oxides in semi interpenetrating polymeric networks alginate/poly(N-isopropylacryl amide) is analyzed [12]. Review [13] describes in detail polymeric composites containing nanodispersed magnetic iron oxides as well as manifold perspectives of their use as magnetic storage media, contrast agents in magnetic resonance imaging (MRI), for targeted drug delivery and destruction of tumor tissue under the action of high-frequency magnetic fields ("intercellular hyperthermia"), and other medical applications, biosensing, bioseparations, etc. In particular M. Eid [14] demonstrated the efficiency of using in oncology of hydroxyethylmethacryate-agar and -gelatin hydrogels incorporating nanodispersed magnetite prepared by gamma irradiation. Similar biocompatible magnetite-polyacrylic acid-type hydrogel was prepared and used by G. Bardajee [15]. Magnetic nanocomposites were also based on styrene copolymers with acrylic acid [16] and polyaniline-polycarbazole matrix [17]. Beside magnetite, another magnetic iron oxide, maggemite γ-Fe_2O_3, in the form of ~100 nm particles, can be dispersed in a polymeric matrix, e.g. cross-linked cyclodextrine as shown by Z. Ghorbani [18].

In the present paper, structure of magnetic nanoparticles is investigated in spherical beads of homogeneous hypercrosslinked polystyrene material CPS(0.3)-100E based on gel-type styrene-0.3 % DVB copolymer [19], in beads of biporous hypercrosslinked MN200 (Purolite Int., U.K.) having micro- and macropores with radii of ~0.7 nm and ~50 nm, respectively [20], as well as beads of polydivinylbenzene-type mesoporous (5–7 nm) material Amberlite XAD-4 (Rohm&Haas, USA). Magnetic nanoparticles form within the above polymer matrixes as the result of chemical precipitation of iron hydroxide followed by its transformation to magnetite. This simple approach to magnetite nanoparticles was previously used e.g. in [14, 15], where polymeric hydrogels were soaked with aqueous solutions of Fe(II) and Fe(III) and then treated with ammonia.

Magnetic materials prepared on the bases of the above polystyrene-type materials are denoted as MCPS(0.3)-100E, MMN200 and MXAD-4, respectively. Some of the thus prepared haemocompatible magnetic sorption materials [21] were earlier shown to prove useful in therapeutic treatment of blood of sepsis patients [22].

Experimental

1. Materials and reagents

Styrene was subjected to vacuum distillation. Divinylbenzene (65 % content of *m*- and *p*-isomers) and 2,2′-azo-bis-isobutyronitrile (both of "Merck", Germany) were used without purification. Home-prepared monochlorodimethyl ether (MCDE) was distilled, collecting the fraction that boils in the temperature range from 57 to 61 °C (refraction index n^{20}_D=1,394).

2. Synthesis of hypercrosslinked polystyrene networks

Hypercrosslinked microporous networks examined in this work have been obtained by an extensive crosslinking of polystyrene chains in a 10 % solution of a technical linear polystyrene (M_w=300,000) in ethylene dichloride (polymer LPS-100E) or in the ultimately swollen slightly crosslinked gel-type styrene-divinylbenzene copolymer beads (0.3 and 0.6 % DVB) in the presence of $SnCl_4$ by means of monochlorodimethyl ether [19]. The above initial copolymers were prepared by conventional suspension polymerization of the monomers mixture using 0.6 % (wt) of 2,2′-azo-bis-isobutyronitrile as initiator. The beads obtained were subjected to extraction with toluene and acetone, washed with water and dried at 80 °C. The above copolymers were then ultimately swollen with excess of ethylene dichloride (EDC) and subjected to post-crosslinking by reacting with 0.5 and 1.0 mol of monochlorodimethyl ether using 1 mol of $SnCl_4$ per 1 mol of the cross-agent to arrive at samples CPS(0.3)-100E, CPS(0.6)-100E and CPS(0.6)-200E, respectively. The transparent beads obtained were washed with acetone, 0.5 N HCl, water, extracted with acetone, finally washed with water and dried at 85 °C for 48 h. According to the element analysis, the networks crosslinked with 0.5 and 1.0 mol of MCDE contained no more than 0.5 and 1.5 % of unreacted residual chlorine (in the form of pendant chloromethyl groups).

The above Friedel-Crafts type reaction of one molecule of MCDE with two phenyl groups belonging to two different polystyrene chains results in the formation of a $–CH_2–$ link between the phenyls, i.e. of a rigid diphenylmethane-type bridge between the chains. The polymers crosslinked with 0.5 mol of the bifunctional crosslinking reagent, MCDE, namely, polymers CPS(0.3)-100E, CPS(0.6)-100E, have the calculated degree of crosslinking of 100 %, meaning that each phenyl ring of polystyrene chains is involved into formation of a cross-bridge. For the networks crosslinked with 1.0 mol of MCDE, the formal crosslinking degree amounts to 200 % since two methylene bridges now substitute each phenyl ring, thus giving sample CPS(0.6)-200E. In these abbreviations, the first and the second numbers denote the content of DVB in the initial copolymer and the degree of final crosslinking (100 or 200 %), respectively.

3. Preparation of magnetic sorbents.

For introducing iron hydroxide nanoparticles into the above neutral polymers, the latter were soaked with a mixed solution of suitable salts of Fe(II) and Fe(III) in a suitable

solvent (that wets the surface of the beads and penetrates into their pores), and then treated with aqueous ammonia. In the case of bi-porous polymer MN200, 20 g of beads were provided with a hot (~50 °C) aqueous solution of a mixture of $FeCl_3$*$6H_2O$ (14.5 g) and $FeSO_4$*$7H_2O$ (14.5 g) in 44 ml H_2O and left for 24 h. Then the beads were separated from the solution on a glass filter and transferred into a beaker with 62 ml 10 % aqueous ammonia. After 24 h the polymer was thoroughly washed with water and dried at 90 °C in an inert atmosphere to constant weight. Alternatively, for the microporous CPS(0.3)-100E and mesoporous XAD-4 which are badly wetted with aqueous solutions, bead samples (2 g) were covered with hot (~50 °C) solution of $FeCl_3$*$6H_2O$ (0.6 g) and $FeCl_2$*$4H_2O$ (0.44 g) in 6 ml ethanol. Again, after 24 h the beads were separated, transferred into 10 % aqueous ammonia (6 ml), washed and dried according to the above protocol.

Naturally, both the concentration of iron salts solution and after-treatment procedures determine the amount of iron oxide introduced, size of its particles and properties of the final nanocomposite. In a series of experiments it has been found that composite materials with specific magnetization of no less than 4 G cm^3 g^{-1} (acquired in a magnetic field of a rather weak permanent magnet) and still preserving acceptable adsorption properties should incorporate 12–14 wt.% Fe_3O_4, i.e. 9–10 % Fe (Table 1).

4. Measurements

Apparent inner surface area, S_{in}, was determined by low temperature sorption of argon from its specified mixture with helium, followed by thermal desorption of argon in a modified gas-chromatographic system, and calculated according to single-point BET method.

Swelling of polymers (maximum solvent uptake) was determined by weighing first the dry and then the swollen sample. The excess solvent was removed from the swollen beads by centrifugation at 4,000 rpm for 15 min in a tube with a porous bottom.

The apparent density, d_{app}, of the polymers was calculated after measuring diameters of 70 to 100 polymer beads (using microscope with a precision of ±0.001 mm) and then measuring their total weight. Only defect less spherical and transparent beads were taken for the measurements. Repeating the procedure 4 times showed the reproducibility of determining d_{app} to be better than ±5%.

For electron microscope investigations, the iron oxide-containing polymer composites in the form of finely disintegrated beads (using an agate mortar) to peaces of less than 1 μm in size were examined in a LEO912 AB OMEGA transmission electron microscope. The main parameters of the microscope were as follow: accelerating voltage, 60, 80, 100, 120 kV; illumination area, 1–75 μm; illumination aperture, 0.02–5 mrad; magnification, 80× to 500000×; image resolution, 0.2–0.34 nm; resolution according to the energy of non-elastic scattering, 1.5 eV; capture range for the energy of non-elastic scattering, 0–2,500 eV. Average size and size distribution of magnetite nanoparticles was estimated from micrographs of 8 to 10 polymer micro fragments by examining 170 to 300 individual nanocristallic species. As a rule, they were shaped as regular hexagons.

An AMUR-K SAXS diffractometer was used to collect scattering data from the samples of hypercrosslinked polystyrenes and nanocomposites based on them. The diffractometer was equipped with a linear position-sensitive detector OD3 covering the angular range $0.1<s<10.5$ nm^{-1} ($s=4\pi \sin\theta/\lambda$ is the modulus of the scattering vector, 2θ being the scattering angle), and a Kratky collimation system. The wavelength used was $\lambda=0.1542$ nm (CuK_α line of a long-fine focus tube with a copper anode, pyrolytic graphite monochromator). The X-ray beam cross section was 0.2×8 mm. The measurements were corrected by the collimation effects.

Specific magnetization of the composites was determined at room temperature using a vibrating sample magnetometer in a magnetic field of 2.5 kGs.

Iron content of nanocomposites was determined using a roentgen fluorescence spectrometer VRA-30 (Carl Zeiss, Germany).

Results and discussions

Physical properties of polymer sorbents

The techniques used in present work for introducing iron hydroxide into the polymer matrix and converting it into magnetic nanoparticles allows obtaining magnetic adsorbing composite materials from both microporous and biporous starting polymers, the latter matrixes containing micro- and macropores. In the first case, beads acquire a dark color, but remain optically transparent (Fig. 1a and b), though loose a significant portion of the uptake capability with respect to water and organic solvents. For the biporous matrixes, sorption of water, toluene and ethanol remained on the initial high level (Table 1).

Main properties of the initial polymers and magnetic composites derived from them are summarized in Table 1>.

All composites examined incorporate 9–10 wt.% iron in the form of magnetic oxides and, therefore, acquire magnetic properties in a weak magnetic field of a permanent magnet (Fig. 2a, b). Specific magnetization values for the both microporous and biporous types of composites are comparable - from 4 to 6.8 G cm^3 g^{-1} (Table 1).

Sorption properties of magnetic adsorption materials, in comparison with those of initial polymers, have been studied under static conditions in saturated vapors of iodine and several toxic organic and metal organic compounds. It turned

Table 1 Physical properties of polymer sorbents and magnetic nanocomposites on their basis

Polymer	Fe (wt%)	S_{in} (m^2 g^{-1})	d_{app} (g cm^{-3})	Specific magnetization (G cm^3 g^{-1})	Maximum absorption (ml g^{-1})			Volume swelling degree
					Water	Toluene	Ethanol	Ethanol
CPS(0.3)-100E	–	1,000	0.72	–	1.20	2.70	2.70	2.42
MCPS(0.3)-100E	9.8	200	1.05	4.0±0.8	0.40	1.06	0.97	1.60
MN200	–	1,100	0.48	–	1.54	1.92	1.91	1.17
MMN200	8.8	1,200	0.55	6.8±1.4	1.30	1.31	1.38	1.16
XAD-4	–	800	0.52	–	1.05	1.54	1.51	1.16
MXAD-4	9.4	1,200	0.61	5.2±1.0	0.74	0.88	0.85	1.06

out that the introduction of nanoparticles of iron oxide in the amount of 12–14 wt.% into hypercrosslinked polystyrene beads of both microporous and biporous structure does not reduce noticeably their excellent sorption performance. This is evident from Fig. 3 which depicts sorption dynamics of iodine vapors. Herewith, the biporous sample MMN-200 exhibits sorption capacity almost twice as high as that of the microporous MCPS(0.3)-100E, just like the two parent intact polymers. For that reason, further tests were performed with the first material, the more that it is based on the industrially available hypercrosslinked polystyrene MN-200.

Though the sorption dynamics, when estimated by the static technique used, does not permit calculating any kinetic parameters since the rate of vapor uptake in a closed volume strongly depends on the shape of the beads sample (whether beads are spread in a thin layer on a permeable surface or packed into a small bawl), still, comparing different sorbates under identical conditions gives an idea not only about the absolute value of sorption but also about the relative rates of sorption. Sorption equilibrium was attained rather quickly, within 2–4 h, in the case of toxic hexacarbonyl chromium and cyclopentadienyl mangane tricarbonyl (Fig. 4). Much slower (within 6–8 h) and less efficiently absorbs organic toxicant chloropicrin. Iron pentacarbonyl, obviously decomposes on the air with depositing metallic iron on the pore surface of beads, the weight of the magnetic polymer continues to increase even after 80 h, where the weight of the sample almost doubled.

From these experiments, it should be evident that magnetic adsorbing materials could be applied for efficient removing of e.g. radioactive iodine vapors or other toxic vapors by spreading the material over contaminated surfaces and collecting the sorbent again by means of magnets.

Differential thermal analysis and X-ray diffraction technique examination of iron oxides

During the conversion of iron salts introduced into the initial polymer matrix to oxides by treating the salt-soaked beads with an alkaline aqueous solution, a certain part of salts leaks from the small beads and forms a precipitate from the interstitial liquid. This precipitate was collected, dried and examined by differential thermal analysis technique. Figure 5 shows an express exothermal effect at 560–565 °C on the thermogram, which obviously corresponds to the phase transition of 2nd kind (ferrimagnetic→paramagnetic) characteristic of magnetite (Fe_3O_4) with a Curie-temperature of 580 °C. In the case that the oxide precipitate was oxidized by hydrogen peroxide prior to thermal analysis, the exothermal effect shifted to a higher temperature range of about 670 °C. This

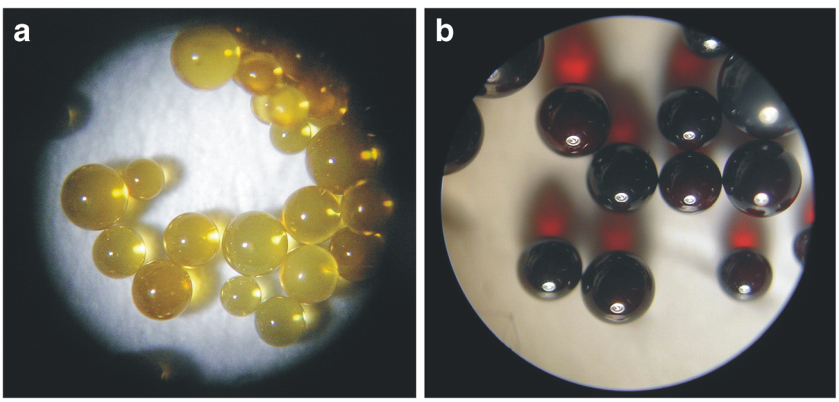

Fig. 1 Initial microporous hypercrosslinked polymer CPS(0.3)-100E (**a**) and nanocomposite beads MCPS(0.3)-100E on their basis (**b**)

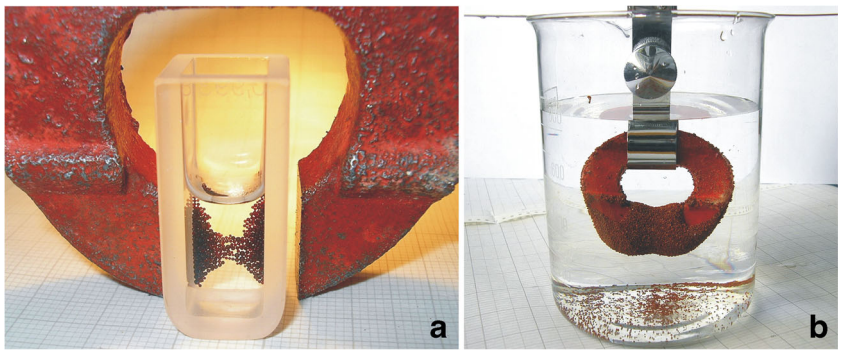

Fig. 2 Magnetic composite beads in an aqueous suspension placed between poles of a permanent magnet. Microporous (**a**) and biporous (**b**) materials

effect is characteristic of the phase transition of maggemite→gematite (α-Fe_2O_3) at 675–680 °C; maggemite being formed on oxidation of magnetite ($Fe_3O_4 \rightarrow \gamma$-$Fe_2O_3$). These data imply that nanoparticles formed within the polymer beads are represented by ferromagnetic magnetite.

This suggestion could find corroboration on examining the parent and magnetic polymer using X-ray diffraction technique. Diffractogramm of the initial polymer consists of two very broad scattering bands at 10 and 20° which correspond to amorphous structure of hypercrosslinked polystyrene. Magnetic nanocomposites exhibit, in addition to the above bands, a series of peaks having indexes 220, 311, 400, 422, 511, 440 (Fig. 6). Identification of this series by comparing their positions and relative intensities with literature data for various iron oxides, unambiguously testifies for the presence of nanocrystalline magnetite Fe_3O_4 phase within the polymer matrix [23]. Similar diffraction patterns were characteristic of commercial magnetite (nano-sized iron(II,III) oxide, Fe_3O_4 from Sigma Aldrich, USA, 98 % pure) presented by Haldar [17], as well as magnetite prepared by Shen [24] through thermal treatment of $FeCl_3$ dissolved in ethylene glycol. Other types of iron oxides, if present at all, do not display their characteristic reflexes in the diffraction pattern in noticeable amounts. The most intensive diffraction peak for magnetite having index (311) is observed at the scattering angle of 35.4. When calculated from the width of this reflex in accordance with the Selyakov-Sherrer equation, the effective radii of magnetite nanocrystallites amounted to ~3, 5 and 8.5 nm in products MCPS(0.3)-100E, MXAD-4 and MMN200, respectively.

Studying the microstructure of the MCPS(0.3)-100E nanocomposite by transmission electron microscopy gave a similar result of 4±1 nm for the radius of iron oxide nanoparticles [25].

In the present work, we subjected the initial polymeric materials and the final magnetic nanocomposites to a detailed examination by small-angle X-ray scattering. Preliminary results appeared in the previous study [23].

First of all, the non-porous gel-type copolymer of styrene with 0.6 % DVB (SD0.6) was examined, which was the starting material for the hypercrosslinking procedure to give samples CPS(0.6)-100E and CPS(0.6)-200E, depending on the formal crossinking degree, 100 and 200 %, respectively. For comparison, another hypercrosslinked network, LPS-100E, was prepared from a concentrated solution of linear polystyrene of molecular mass 300 kDa. Diffraction patterns

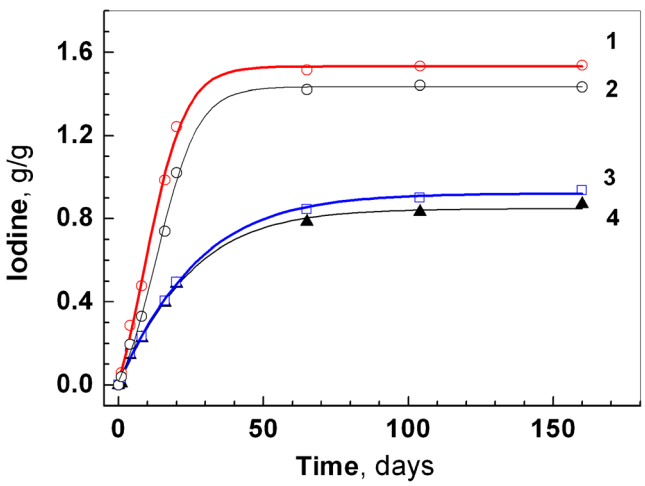

Fig. 3 Sorption dynamics of iodine vapors at room temperature (20–22 °C) by MN-200 (1), magnetic sorbent MMN-200 (2), polymer CPS(0.3)-100E (3) and magnetic material MCPS(0.3)-100E (4)

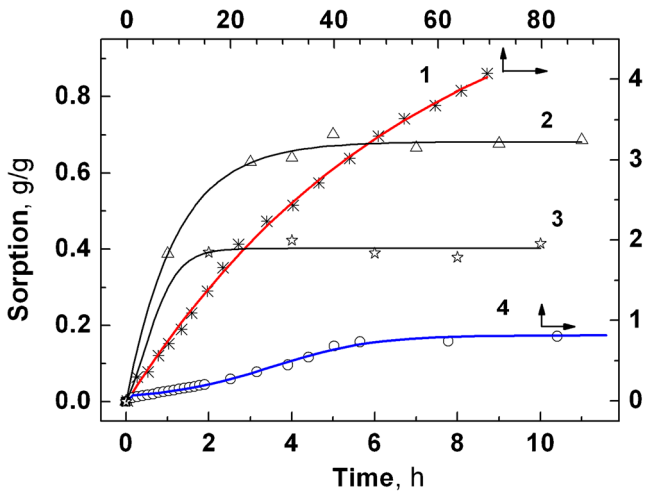

Fig. 4 Sorption dynamics on magnetic MMN-200 of iron pentacarbonyl (1), cyclopentadiene mangan tricarbonyl (2), chromium pentacarbonyl (3), and chloropicrin (4)

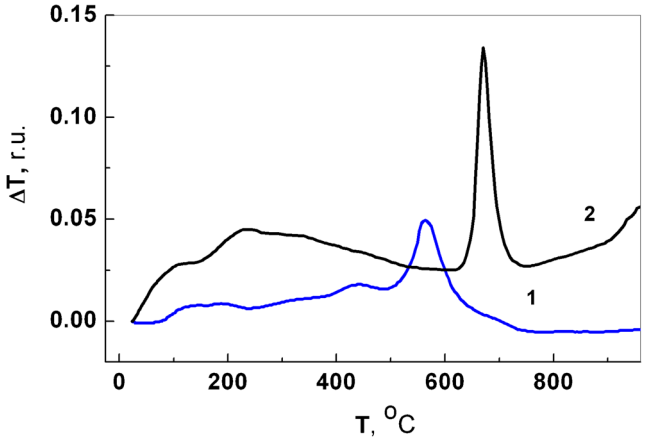

Fig. 5 Differential thermal analysis of iron hydroxide precipitates isolated from the interstitial liquid during the preparation of MMN-200 (1) and of material obtained by oxidation of this precipitate with H_2O_2 (2)

of these polymers are presented in Fig. 7. In addition to the dry state, the hypercrosslinked sample CPS(0.3)-100E was also examined in swollen states equilibrated with water and tetradecane, as well as saturated with iodine vapors (Fig. 8).

As known for "gel-type" microporous hypercrosslinked polymers, sample CPS(0.3)-100E increases noticeably its volume on saturation with water and, particularly, with organic solvents like polar ethanol (see Table 1) or less polar iodine and tetradecane. Experimental dependencies of scattering intensity on the observation angle (Figs. 7 and 8) do not display any extended linear range, which would testify to the presence of a certain favorite size of pores or heterogeneity in electronic density within the polymer structure. Rather, the scattering pattern corresponds to a statistic size distribution of density fluctuations in their friable, but rigid continuous networks. At the same time, linear parts can be seen on scattering charts for magnetic MMN200 (Fig. 9) and especially microporous MCPS(0.3)-100E (Fig. 10). They definitely correspond to a rather narrow size distribution of magnetite nanoparticles.

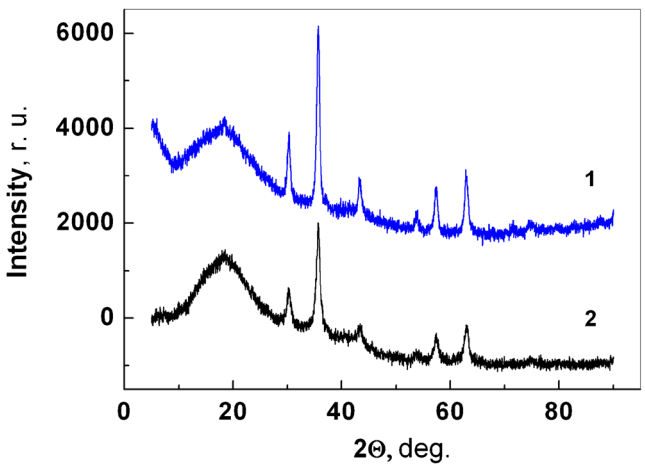

Fig. 6 X-ray powder diffraction of nanocomposites MMN200 (1) and MXAD-4 (2)

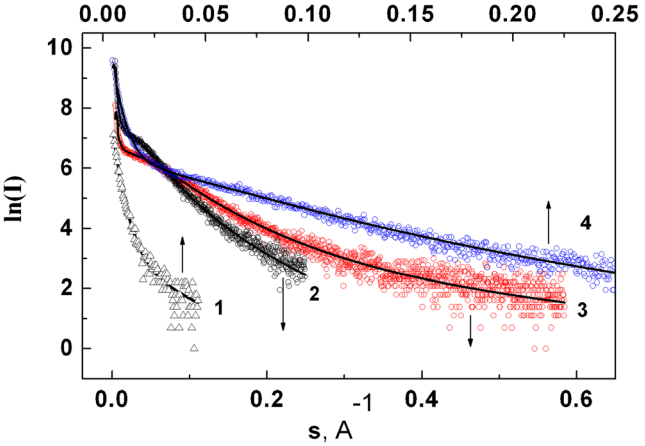

Fig. 7 Experimental small-angle scattering intensities and the theoretical fitting lines with optimized parameter values for dry non-porous copolymer SD0.6 (1) and hypercrosslinked polystyrene samples LPS-100E (2), CPS(0.6)-200E (3), CPS(0.6)-100E (4)

General scheme of theoretical treatment of intensity pattern of small-angle X-ray scattering from a multicomponent polydisperse system

A detailed analysis of the size distribution of scattering heterogeneities in a multicomponent polydisperse system was performed by using the approach described in the previous study [26]. Scattering intensity from a polydisprse system of noninteracting spherical particles was represented as sum of K components, each described by the Schultz distribution of radii R

$$D_k(R) = G(R, R_{0k}, \Delta R_k) = \left(\frac{z+1}{R_{0k}}\right)^{z+1} \frac{R^z}{\Gamma(z+1)} \exp\left[-\frac{(z+1)R}{R_{0k}}\right], \quad (1)$$

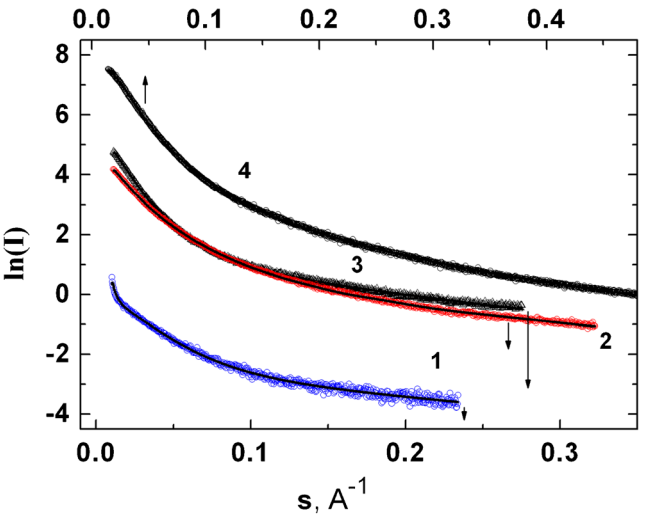

Fig. 8 Experimental small-angle scattering intensities and the theoretical fitting lines with optimized parameter values for the hypercrosslinked polystyrene CPS(0.3)-100E saturated with iodine (1), tetradecane (2), water (3) and in dry state (4)

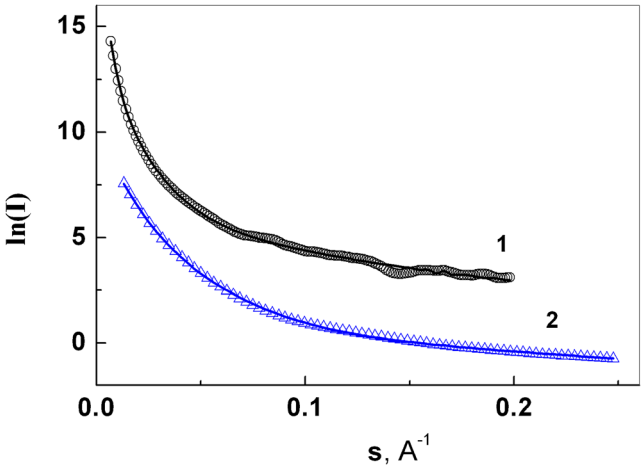

Fig. 9 Experimental small-angle scattering intensities and the theoretical fitting lines with optimized parameter values for the hypercrosslinked polystyrene biporous sample MN200 (1) and magnetic nanocomposite MMN200 (2) based on it

where $k=1,\ldots,K$; unknown parameter $z=(R_{0k}/\Delta R_k)^2-1$ depending on the sought model parameters, mean radius R_{0k} and the distribution width ΔR_k. The scattering intensity from the k-th component is an isotropic function

$$I_{k0}(s) = \int_0^\infty D_k(R) v_k(R) [\Delta\rho_k(R)]^2 i_{0k}(s,R) dR, \qquad (2)$$

where $v_k(R)$ is the particle volume, $\Delta\rho_k(R)$ is its scattering contrast (the difference between mean electron densities of the particle and the media), $i_{0k}(s,R)$ is the particle scattering intensity. The model assumptions made here were that $K=2$–3,

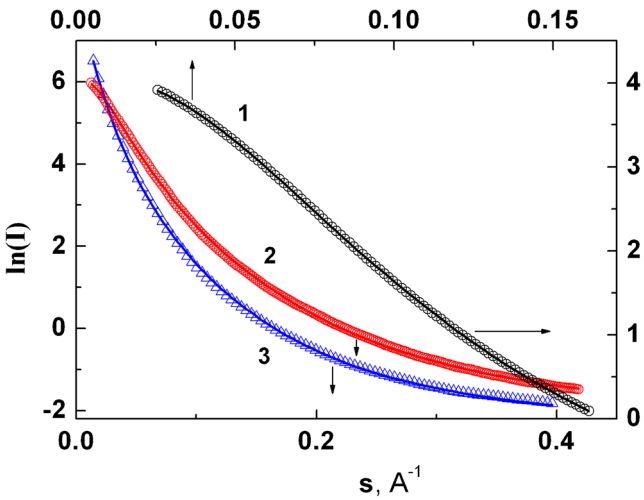

Fig. 10 Experimental small-angle scattering intensities and the theoretical fitting lines with optimized parameter values for the nanocomposite MCPS(0.3)-100E (1) based on microporous copolymer SD0.3, hypercrosslinked polystyrene CPS(0.3)-100E (2), and composite MXAD-4 (3)

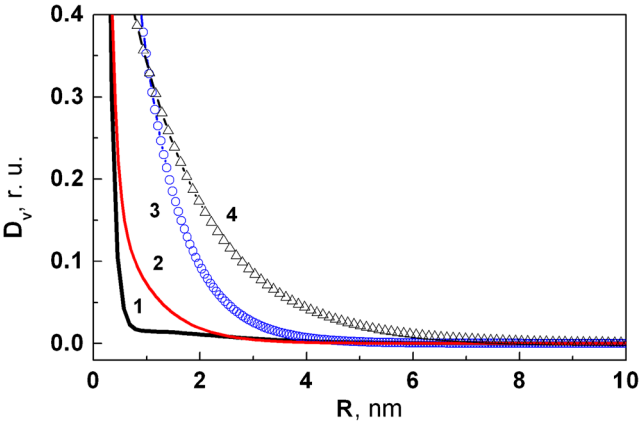

Fig. 11 Calculated size distribution of heterogeneities in the polymer SD0.6 (1) and hypercrosslinked samples CPS(0.6)-200E (2), CPS(0.6)-100E (3) and LPS-100E (4)

all the particles (or inhomogeneities) are spherical ($i_{0}(s,R)=\{[\sin(sR) - sR\cos(sR)]/(sR)^3\}^2$, $\nu_k(R)=3.14\,(4/3)R^3$) and their contrast equals unity. The last approximation does not influence the shape of the size distribution which was the matter of the analysis. The upper limit of integration in (2) was chosen such as to provide the remainder to be less than 10^{-3} at all angles. The sum of K components should represent the experimental intensity

$$I(s) = \sum_{k=1}^{K} V_k I_{k0}(s), \qquad (3)$$

with the relative contributions V_k which are also the sought model parameters. The search of model parameters was performed using the program POLYMIX which utilizes the NL2SOL algorithm [27] for solving the least-squares problem of minimization of the sum of squared discrepancies between

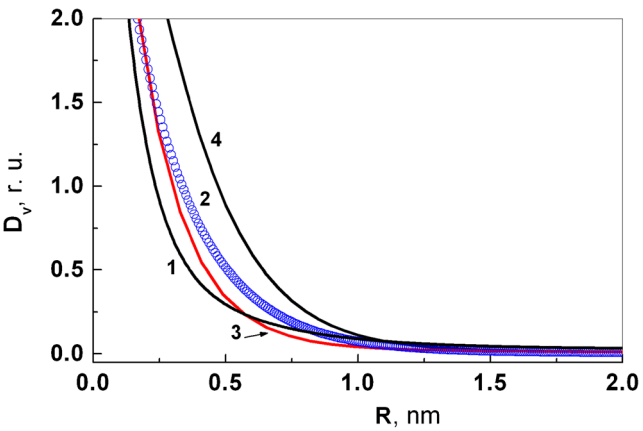

Fig. 12 Calculated size distribution of heterogeneities in the hypercrosslinked sample CPS(0.3)-100E when saturated with water (1) and iodine (2), in dry state (3), and swollen with tetradecane (4)

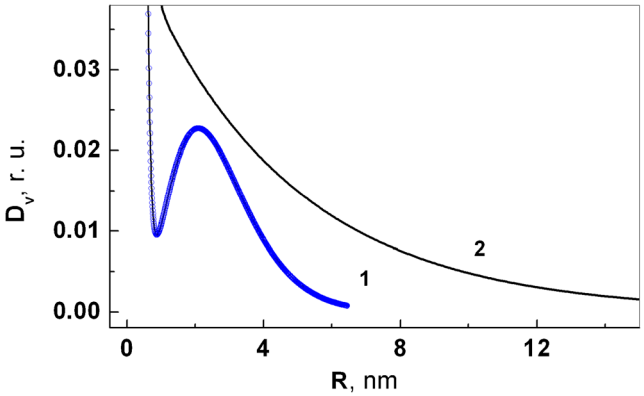

Fig. 13 Calculated size distribution of heterogeneities in the nanocomposite MCPS(0.3)-100E (1) based on hypercrosslinked sample CPS(0.3)-100E and nanocomposite MXAD-4 (2) based on mesoporous polymer XAD-4

the experimental and model scattering intensities as described in the previous study [26].

Figures 11, 12, 13 and 14 present the size distribution of volumes of structural heterogeneities in the polymer and nanocomposite samples under examination, which were calculated from their SAXS patterns in accordance with the above logical scheme and program "POLYMIX". On vertical axes, there are plotted volume portions (Dv) of heterogeneities of a given radius, related to the total sum of volumes (which is the total surface under the Dv(R) curve), under assumption that the heterogeneities possess spherical shape.

For the microporous hypercrosslinked polystyrenes CPS(0.6)-200E, CPS(0.6)-100E and LPS-100E (Fig. 11), characteristic appears to be a rather smooth distribution of volumes of scattering heterogeneities of the electron density of the matrix within the range of up to 5–6 nm, with predomination of smaller pores of less than 1–2 nm in radius. Average size of heterogeneities

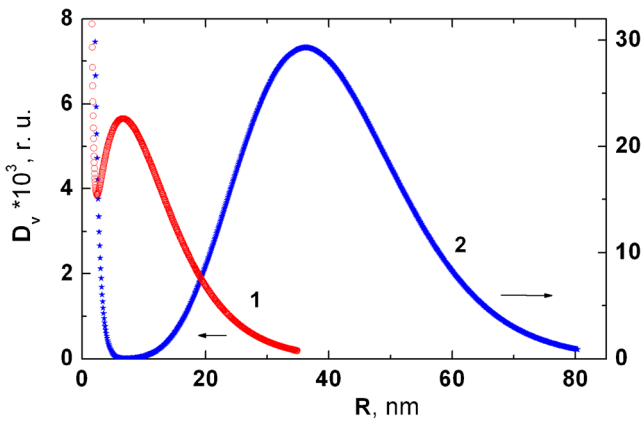

Fig. 14 Calculated size distribution of heterogeneities in the nanocomposite MMN200 (1) and initial biporous hypercrosslinked polymer MN200 (2)

Table 2 Effective radii of magnetite nanoparticles formed in polymer matrixes of various structure

Polymer	XRD R (nm)	SAXS Maximum distribution (nm)	TEM
MCPS(0.3)-100E	3	2.1	3.5
MMN200	8.5	6.7	7.4
MXAD-4	5	[a]4.4	10.5

[a] Calculated for "center of gravity" of distribution plot according to POLYMIX program

increases in the above sequence of hypercrosslinked materials. The non-porous gel-type SD0.6 copolymer, the starting material for the synthesis of hypercrosslinked CPS(0.6) series, is really homogeneous and does not display density fluctuations of over 0.5 nm in radius. Heterogeneities observed in hypercrosslinked materials should be associated with their micropores, since positronium annihilation techniques also reveal voids with radii less than 1–2 nm in these polymers [28]. Saturation of the polymer CPS(0.3)-100E with water or iodine (uptake ~1 g/g) does not change significantly the size of observed heterogeneities, the sorbates being evenly "dissolved" within the polymer matrix. Saturation with tetradecane (~2 g/g) causes a certain expansion of the network (Fig. 12).

Figure 13 presents plots of size distributions of scattering density fluctuations from the iron-containing nanocomposites MCPS(0.3)-100E and MXAD-4, calculated according to Schulze for two partial distributions in the ranges of $R<\sim0.5$ nm and $R>\sim0.5$ nm. One immediately can notice a preferred size around $R\sim3$ nm for the density fluctuations in the microporous hypercrosslinked composite sample MCPS(0.3)-100E. They should be attributed to magnetite microparticles in this nanocomposite. Diameters of mineral nanoparticles presented in Table 2 were estimated for this sample from the partial distribution within the mode of $R>\sim0.5$ nm. For the nanocomposite MXAD-4 based on mesoporous Amberlite XAD-4, size distribution looks to be rather smooth, so the average size of nanoparticles was estimated for the "center of gravity" of exponential distribution within the partial mode $R>\sim0.5$ nm. Figure 10 makes it possible to compare average sizes of density fluctuations in the nanocomposite MMN200 with that in the initial biporous hypercrosslinked polymer MN200. Whereas radius of magnetic particles formed within the pores is small (6.7±3.8 nm), the average size of pores is rather large (36±7 nm). One notes that, estimated by volume, macropores make the largest contribution to this value for the biporous polymer. This result seems to agree with the average size of pores of circa 50 nm in MN200 determined by BET nitrogen sorption technique [20].

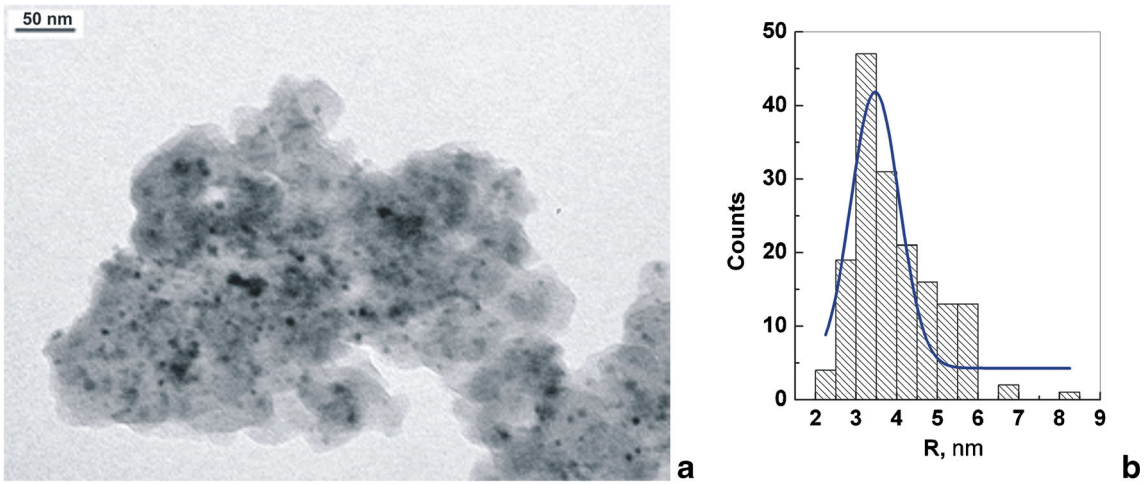

Fig. 15 Transition electron micrograph (bench mark - 50 nm) of a nanocomposite MCPS(0.3)-100E fragment (**a**); histogram and differential function of magnetite nanoparticles size distribution (**b**) (170 particles from 10 nanocomposite fragments)

In general, the above discussed results of examining structures of polymeric materials confirm the earlier made suggestion [29] of a rater smooth statistical size distribution of structural elements in hypercrosslinked networks, resulting in a system of "nanopores" which radius does not exceed 2–2.5 nm for the sample CPS(03)-100E. Increasing the formal crosslinking density to 200 % results in further decrease of pore size to les than 1.5–2 nm (Fig. 11). Hypercrosslinked material LPS-100E prepared through intensive crosslinking of linear polystyrene displays larger heterogeneities of up to $R \sim 5$–6 nm, which can reflect heterogeneities caused by individual macromolecular coils in the initial concentrated polystyrene solution. It has been noticed rather early [29] that cleavage surfaces of hypercrosslinked materials based on styrene-DVB copolymers exhibit in electron microscopy no supramolecular structures, whatsoever, while morphological pictures of products of hypercrosslinking linear polystyrene solutions display some spherical nanostructures. The industrial "biporous" product MN200 contains much larger transport pores, in addition to the plurality of nanopores inherent to the hypercrosslinked networks. The transport pores were intentionally introduced into this sorbent structure, in order to enhance the mass transfer kinetics.

Magnetic nanoparticles obviously form in the largest voids of networks due to the ripening process of iron hydroxide precipitates during the crystallization of magnetite. Therefore, the average size of magnetite nanoparticles amounts to 2.1±0.6 nm in MCPS(0.3)-100E and reaches 6.7±3.8 nm in MMN200 at the iron content of about 10 and 9 %, respectively.

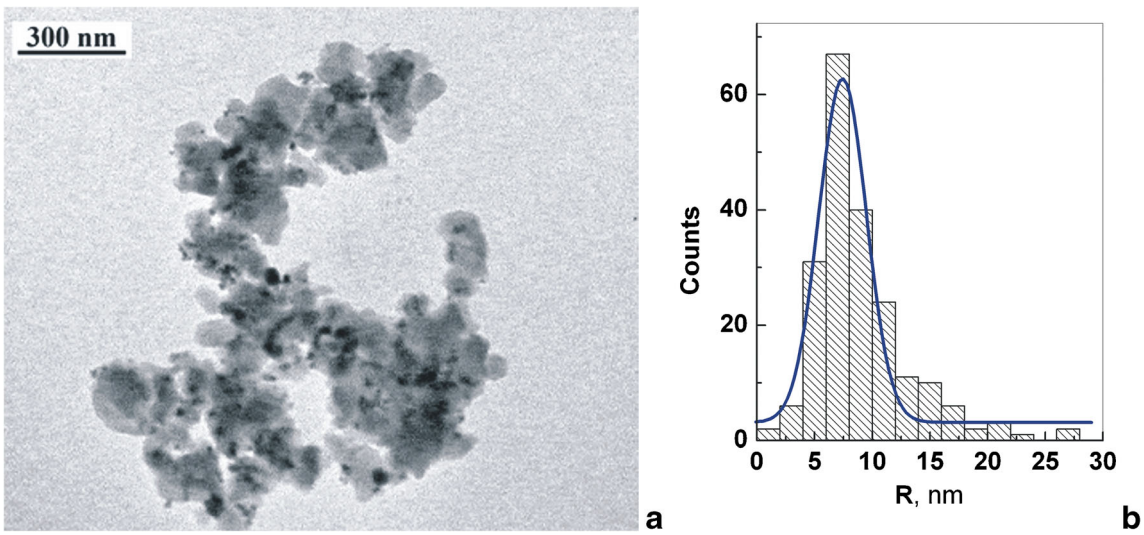

Fig. 16 Transition electron micrograph of a nanocomposite MMN200 fragment (**a**); histogram and differential function of magnetite nanoparticles size distribution (**b**) (200 particles from 12 nanocomposite fragments)

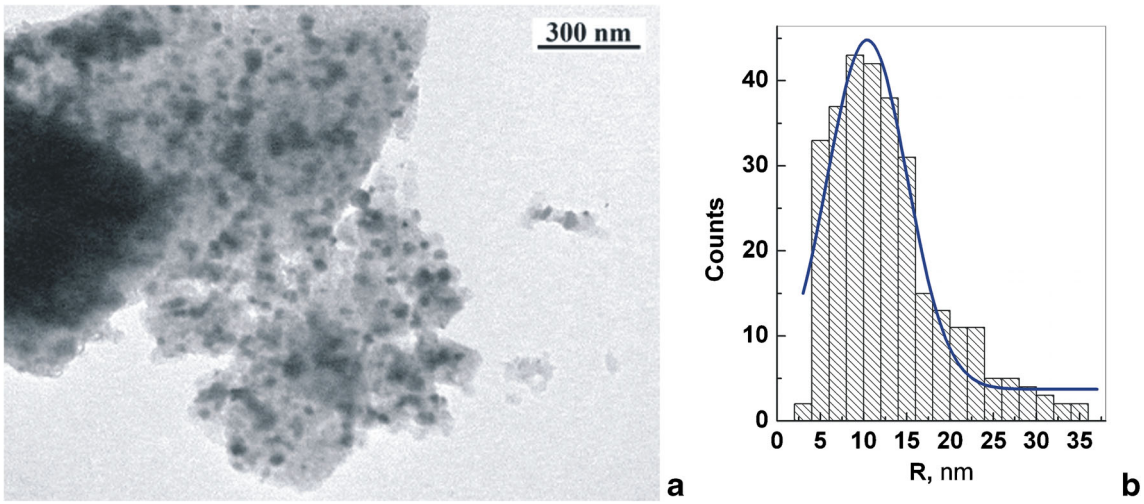

Fig. 17 Transition electron micrograph of a nanocomposite MXAD-4 fragment (**a**); histogram and differential function of magnetite nanoparticles size distribution (**b**) (300 particles from 8 nanocomposite fragments)

Transition electron micrography of nanocomposites

When in dry state, beads of hypercrosslinked polymers as CPS(0.3)-100E, MN200, XAD-4 and iron oxide incorporating nanocomposites based on them easily disintegrate in agate mortar. Herewith nanoparticles of iron oxide remain within the submicron-sized polymer fragments.

Due to the large difference in the density of magnetite nanoparticles and the hypercrosslinked polystyrene matrix-type environment, the nanoparticles become visible in transition electron microscopy. Indeed, Figs. 15a, 16 and 17a exhibit magnetite inclusions in the form of dark spots.

Compared to the above results of X-ray diffraction, the maximum of particle size distribution curves for the same samples MCPS(0.3)-100E and MMN200 estimated by TEM technique positions at a slightly larger values of $R \sim 3.5$ and 7.4 nm (Figs. 15b, 16b), respectively. This is rather logical, because the smallest particles escape registration during the automatic optical analysis of the image, while visible particles appear larger due to the unsharpness of their contours. Besides, associates and overlapping shadows may appear on micrographs as single species. Table 2 compares magnetite particle sizes when estimated by using three different techniques, TEM, SAXS, and X-ray diffraction (XRD) analysis [23, 25]. The agreement of data can be considered to be rather satisfactory, so that all above techniques may prove useful, though microscopy generally gives overestimated size values. Strangely, size distribution of magnetite particles formed in the matrix of mesoporous commercial polydivinylbenzene Amberlite XAD-4 was found to be very broad with no preferred mode between 1 and 10 nm in radius (Fig. 13). Mean size of particles can be estimated as ~4.4 nm whereas TEM technique gives for MXAD-4 sample a much larger mean size for the nanoparticles (Fig. 17b).

Using TEM technique for the size evaluation of magnetite nanoparticles formed by the base precipitation of mixed iron (II) and (III) salts within crosslinked agar- and gelatine hydrogels, size maximums at ca 23 nm have been recently found [14], while smaller magnetite particles of 9–12 nm form in the polyacrylate-type hydrogels [15]. Nanoparticles of similar size about 15 nm in diameter in the matrix of biporous hypercrosslinked polystyrene MN200 (Fig. 16a, b), probably, they predominantly locate in the macropores which size may be as large as 100 nm [20]. Within the structurally unique [19] microporous hypercrosslinked polystyrene networks much smaller magnetite nanoparticles of circa 7 nm in diameter (Fig. 15a, b) are stabilized.

Conclusions

Precipitation of mixed iron hydroxides within hypercrosslinked or mesoporous polystyrene-type matrixes opens a way to obtaining magnetic sorption materials that can find application in various specific technologies, due to the easiness of their magnetic separation from alien particulates. Size of magnetite nanoparticles depends on the microstructure of the network and can be easily varied on desire in a vide range from 1 to 10 nm. Average size and size distribution of magnetite nanoparticles can be estimated by several physico-chemical techniques as SAXS, TEM, XRD giving values that satisfactorily agree with each other.

Acknowledgments This work was carried out with the support of Russian Foundation for Basic Research (RFBR) - International cooperation of the Russian-Belarusian research projects 2012–2013, grant № 12-03-90007-Bel_a.

References

1. Pomogailo AD, Rosenberg AS, Uflyand IE (2000) Metal nanoparticles in polymers. Chemistry, Moscow
2. Ambituashta RD, Sillanp M (2010) Water purification using magnetic assistance: a review. J Hazard Mater 180:38–49
3. Marius MS, James PAB, Bahaj AS, Smallman DJ (2005) Development of a highly magnetic iron sulphide for metal uptake and magnetic separation. J Magn Magn Mater 293:567–571
4. Kanayama TOH, Fukui S, Ogawa J, Sato T, Ooizumi M, Terasawa T, Itoh Y, Yabuno R (2008) Application of HTS bulk magnet system to the magnetic separation techniques for water purification. Physica C 468:2128–2132
5. Kuznetsov AA, Filippov VI, Kutushov MV, Komissarova LK, Feldman MG, Kutukova EA, Lenskaya GA (1994) A method of blood purification in an extracorporeal system. Russ Patent 2008929 Pub. Date 15.03.1994
6. Kutushov MV, Kuznetsov AA, Filippov VI (1997) New method of biological fluids detoxification based on magnetic adsorbents. In: Häfeli U, Schütt W, Teller J, Zborowski M (eds) Scientific and clinical applications of magnetic carriers (Proceedings of an international conference on scientific and clinical applications of magnetic carriers, held September 5–7, 1996, in Rostock, Germany). Plenum, New York
7. Kutushov MV (2007) Magnetically operated absorbent and method for the production thereof. US Patent Application Publication 2007/071977 A1 Pub. Date 29.03.2007
8. Sauzedde F, Elaissari A, Pichot C (1999) Hydrophilic magnetic polymer latexes. 1. Adsorption of magnetic iron oxide nanoparticles onto various cationic latexes. Colloid Pol Sci 277:846–855
9. Solntseva DP, Kalinina RN, Krasnov MS, Makarova EI (1998) Method of obtaining of modified sorbent. Russ Patent 2105015 Pub. Date 20.02.1998
10. Leun D, Sengupta AK (2000) Preparation and characterization of magnetically active polymeric particles (MAPPs) for complex environmental separations. Environ Sci Technol 34:3276–3282
11. Kaminski MD, Nunez L (1999) Extractant-coated magnetic particles for cobalt and nickel recovery from acidic solution. J Magn Magn Mater 194:31–36
12. Hernndez R, Sacristn J, Nogales A, Ezquerra TA (2009) Mijangos C. structural organization of iron oxide nanoparticles synthesized inside hybrid polymer gels derived from alginate studied with small-angle x-ray scattering. Langmuir 25(22):13212–13218
13. Philippova O, Barabanova A, Molchanov V, Khokhlov A (2011) Magnetic polymer beads: recent trends and developments in synthetic design and applications. Eur Polym J 47:542–559
14. Eid M (2013) Preparation and characterization of natural polymers as stabilizer for magnetic nanoparticles by gamma irradiation. J Polym Res 20:112
15. Bardajee GR, Hooshyar Z (2013) A novel biocompatible magnetic iron oxide nanoparticles/hydrogel based on poly (acrylic acid) grafted onto starch for controlled drug release. J Polym Res 20:298
16. Wei S, Zhang Y, Xu J (2011) Preparation and properties of poly(acrylic acid-co-styrene)/Fe_3O_4 nanocomposites. J Polym Res 18:125–130
17. Haldar I, Biswas M, Arabinda Nayak A (2012) Preparation and evaluation of microstructure, dielectric and conductivity (ac/dc) characteristics of a polyaniline/polyN-vinyl carbazole/Fe_3O_4 nanocomposite. J Polym Res 19:9951
18. Ghorbani Z, Baharvand H, Nezhati MN, Panahi HA (2013) Magnetic polymer particles modified with β-cyclodextrin. J Polym Res 20:199
19. Pastukhov AV, Tsyurupa MP, Davankov VA (1999) Hypercrosslinked polystyrene: a polymer in a non-classical physical state. J Polym Sci Part B Polym Phys 37:2324–2333
20. Hypersol-MacronetTM Sorbent Resins (1995) Purolite technical bulletin. The Purolite Company, UK
21. Anisimova NY, Dolzhikova YI, Davankov VA, Pastukhov AV, Miljaeva SI, Senatov FS, Kiselevsky MV (2012) Hemocompatibility of nanostructured sorbents based on hypercrosslinked polymers of the styrosorb series. Russ J Biother 11(1):23–27
22. Anisimova NY, Dolzhikova YI, Davankov VA, Pastukhov AV, Miljaeva SI, Senatov FS, Kiselevsky MV (2012) Prospects for the application of biporous sorbents based on hypercrosslinked styrene polymers for the prevention and treatment of systemic purulent-septic complications. Nanotechnologies in Russia 7(5–6):318–326
23. Pastukhov AV, Davankov VA, Volkov VV, Dembo KA, Zubavichus YV, Korlyukov AA, Filatova AG (2009) Magnetic nanocomposites based on hypercrosslinked polystyrenes. Bull Russ Acad Sci Phys 73(4):471–473
24. Shen P, Jiang W, Wang F, Chen M, Ma P, Li F (2013) Preparation and characterization of Fe_3O_4@TiO_2 shell on polystyrene beads. J Polym Res 20:252
25. Pastukhov AV, Davankov VA (2011) Transmission electron microscopy of composite materials based on hypercrosslinked polystyrenes with nanodispersed inorganic compounds. Bull Russ Acad Sci Phys 75(9):1248–1250
26. Svergun DI, Konarev PV, Volkov VV et al (2000) A small angle x-ray scattering study of the droplet–cylinder transition in oil-rich sodium bis-2-ethylhexylsulfosuccinate microemulsions. J Chem Phys 113(4):1651–1665
27. Dennis JE, Gay DM, Welsch RE (1981) Algorithm 573 NL2SOL - an adaptive nonlinear least-squares algorithm [E4]. ACM Trans Math Softw 7(3):369–383
28. Shantarovich VP, Suzuki T, He C, Djourelov N, Kevdina IB, Davankov VA, Pastukhov AV, Ito Y (2004) Positron annihilation in polymers with highly developed specific surface. Mater Sci Forum 445–446:346–348
29. Tsyurupa MP, Pankratov YA, Tsvankin DY, Zhukov VP, Davankov VA (1985) Morphology of macroreticular isoporous styrene polymers "styrosorb". Polym Sci USSR 27(2):377–385